

# Universality of Periodic Oscillation Induced in Side Branch of a T-Junction in Numerical Simulation

Ryuhei Yamaguchi<sup>1\*</sup>, Gaku Tanaka<sup>1</sup>, Tadashi Nakagawa<sup>2</sup>, Atsushi Shirai<sup>2</sup>, Hao Liu<sup>1</sup>, Toshiyuki Hayase<sup>2</sup>

<sup>1</sup>Graduate School of Engineering, Chiba University, Chiba, Japan

<sup>2</sup>Institute of Fluid Science, Tohoku University, Sendai, Japan

Email: \*ryuhei63@gmail.com

**How to cite this paper:** Yamaguchi, R., Tanaka, G., Nakagawa, T., Shirai, A., Liu, H. and Hayase, T. (2017) Universality of Periodic Oscillation Induced in Side Branch of a T-Junction in Numerical Simulation. *Journal of Flow Control, Measurement & Visualization*, 5, 73-85.

<https://doi.org/10.4236/jfcmv.2017.54006>

**Received:** April 20, 2017

**Accepted:** August 20, 2017

**Published:** August 23, 2017

Copyright © 2017 by authors and Scientific Research Publishing Inc.

This work is licensed under the Creative Commons Attribution International License (CC BY 4.0).

<http://creativecommons.org/licenses/by/4.0/>



Open Access

## Abstract

The flow instability through the side branch of a T-junction is analyzed in a numerical simulation. In a previous experimental study, the authors clarified the mechanism of fluid-induced vibration in the side branch of the T-junction in laminar steady flow through the trunk. However, in that approach there were restrictions with respect to extracting details of flow behavior such as the flow instability and the distribution of wall shear stress along the wall. Here the spatial growth of the velocity perturbation at the upstream boundary of the side branch is investigated. The simulation result indicates that a periodic velocity fluctuation introduced at the upstream boundary is amplified downstream, in good agreement with experimental result. The fluctuation in wall shear stress because of the flow instability shows local extrema in both the near and distal walls. From the numerical simulation, the downstream fluid oscillation under a typical condition has a Strouhal number of 1.05, which approximately agrees with the value obtained in experiments. Therefore, this periodic oscillation motion is a universal phenomenon in the side branch of a T-junction.

## Keywords

Flow Instability, Fluid-Induced Oscillation, Numerical Simulation, SIMPLER Method, T-Junction

## 1. Introduction

T-junction is a typical fluid pipe element used in the construction of power plants. Over the past three decades, many experimental and numerical researchers

have investigated laminar flow inside T-junction for relevance in hemodynamics [1] [2] [3] [4].

More recently, the focus in the hemodynamics field has been the flow instabilities induced in a cerebral aneurysm from the perspective of their growth and rupture [5] [6] [7]. Indeed, although the flow instability and the turbulence occur around the cerebral aneurysm, this instability appears in a pulsatile flow, *i.e.* unsteady flow in a proximal vessel. Furthermore, this phenomenon disappears in a distal vessel. The flow instability also appears in the nasal channel and cantilevered flexible plate [8] [9] [10]. However, this flow instability has not necessarily led to strong periodic oscillations; they may appear temporarily and sometimes as weak periodic oscillations.

Brown & Roshko [11] and Tani [12] found that when two parallel flows differing velocity merge, the high-shear-rates at the interface of these flows induce Kelvin-Helmholtz flow instability and that this phenomenon is universal. These findings are based on fluidoscillation and vibration occurring in the dynamics of fluid flows. Oscillations, self-sustaining oscillations and instability have been studied experimentally for flow past a cavity [13] [14], and flow through an axisymmetric stenosed channel [15].

In previous studies of the T-junction [16] [17] [18] [19], we found that a periodic oscillation was induced in the side branch and that the Strouhal number based on variables in the side branch was independent of Reynolds number, flow division ratio and the ratio of the radii of the side branch and trunk. Qualitatively, this implies that at a certain cross-section the oscillation is strongly related to the local flow structure, *i.e.* high-shear-rate flow between two pairs of vortices with the same rotational sense in the cross section immediately downstream of the side branch. Furthermore, in addition to high-shear-rate flow between two vortices, a fluid oscillation is induced along the shearing separation layer where the tangential velocity profile has inflection points with shear rate several orders larger than that further downstream [19]. Subsequently, the mechanism for the flow vibration was clarified from the flow instability of two kinds of high-shear-rate flow with the inflection point in the side branch of the T-junction confirming the universality of the phenomenon.

However, the experimental approach was unable to clarify in detail how the mechanism of the periodic oscillation occurs, *i.e.* the spatial amplification of flow instability and the distribution of wall shear stress (WSS). In the present study, this mechanism is clarified numerically. The mechanism of periodic oscillation induced in the side branch obtained in the experiment was verified in numerical simulation.

## 2. Method

Numerical simulations were performed of flow in a T-junction (**Figure 1**) configured with the same setup as studied in a previous experimental study [18]. The side branch bifurcates at right-angle from the trunk. To examine the

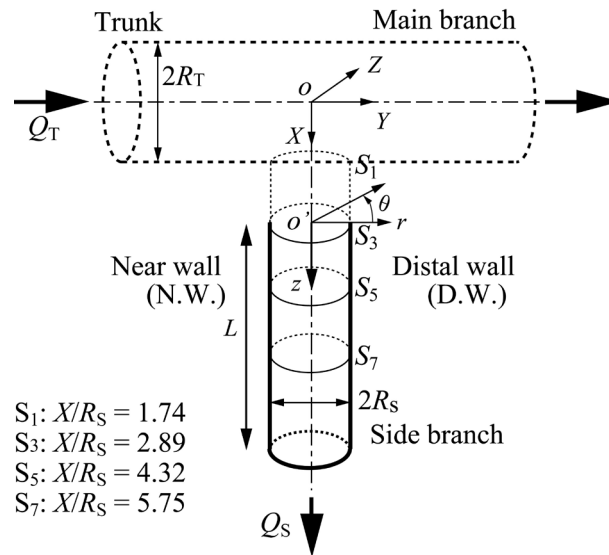


**Figure 1.** Schematic of the T-junction.

universality of the independency for the Strouhal number, a typical setting employed a Reynolds number of  $Re_s = 700$  ( $Q_s/Q_T = 0.50$ ) in the side branch corresponding to  $Re_T = 800$  in the trunk. Also, the tube radius ratio and the flow division ratio were fixed at  $R_s/R_T = 0.57$  and  $Q_s/Q_T = 0.25, 0.33$  and  $0.5$  [18], respectively. The flow division ratio is primarily at  $Q_s/Q_T = 0.5$  because the oscillation frequency is clear at this condition in experiment. Furthermore, in numerical calculation, we examined the spatial amplification of velocity due to flow instability and the distribution of wall shear stress.

The velocity components at 480 numerical grid points in the upper half plane (grid B in **Table 1**) were interpolated from 129 measurement data on a non-uniformly spaced rectangular grid in the  $Y-Z$  plane. The velocity vector field experimentally obtained for a Cartesian coordinate system (**Figure 2(a)**) in a previous study is given as the upstream boundary condition [ $S_3$  in **Figure 3(a)**] [18], where is furthest upstream measurement location for the laser Doppler anemometry. As cylindrical coordinate system is used in the simulation, the velocity in **Figure 3(b)** was interpolated from several points in the Cartesian coordinate system using a staggered grid near the point (**Figure 2(b)**). Specifically, as a grid of cylindrical coordinate in **Figure 2(b)** does not coincide with that of Cartesian coordinate, the velocity component  $\Phi$  at a grid point in cylindrical coordinate using the following equation is interpolated from the surrounding velocities  $\phi_i$  in Cartesian coordinate.

$$\Phi = \frac{\sum_{i=1}^n \left( \frac{1}{d_i^2} \right) \phi_i}{\sum_{i=1}^n \left( \frac{1}{d_i^2} \right)} \quad (1)$$

where  $d_i$  is each distance from the grid in cylindrical coordinate to the surrounding grids in Cartesian coordinate. The numerical domain is  $L = 0.046$  m,

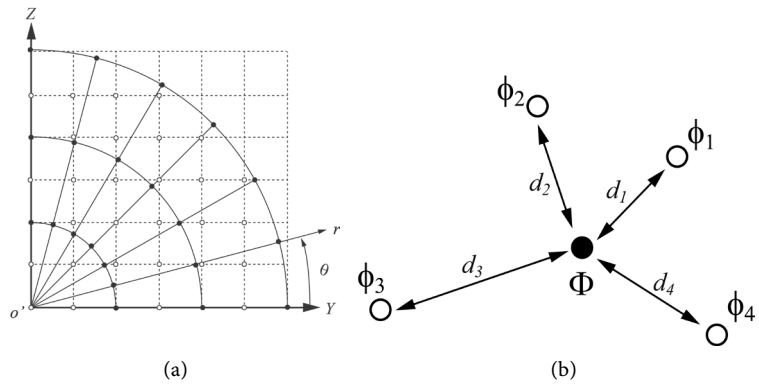


**Figure 2.** (a) Cylindrical and Cartesian grid; (b) Interpolation to simulation data from experiment.

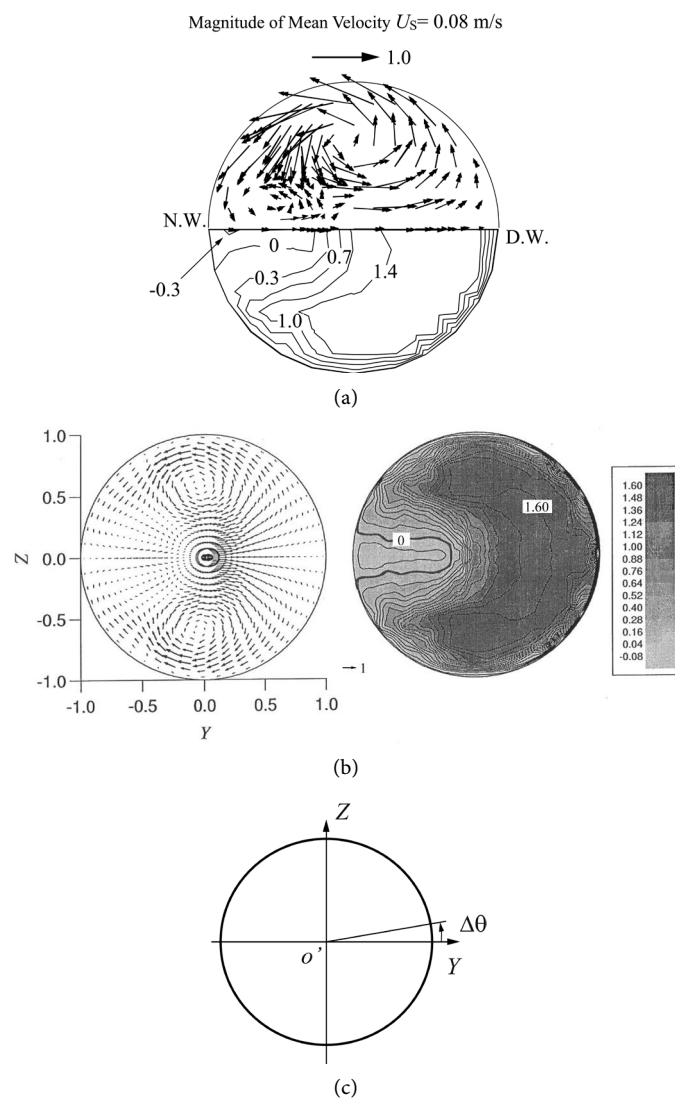


**Figure 3.** Inlet condition and shearing flow at section  $S_3$ . (a) Measured secondary velocity vector plots (upper semicircle) and iso-axial velocity contours (lower semicircle) [18]; (b) Interpolated secondary velocity plots (left) and iso-axial velocity contours (right); (c) Oscillation range in upstream boundary condition.

**Table 1.** Numerical conditions.

	grid A	grid B
Grid points $N_r \times N_\theta \times N_z$	$10 \times 24 \times 24$	$20 \times 48 \times 132$
Grid spacing $h_r \times h_\theta \times h_z$	$0.1 \times \frac{2\pi}{24} \times 0.1$	$0.05 \times \frac{2\pi}{48} \times 0.05$
Time step $\Delta t$	0.1	0.01
Total residual at convergence $\varepsilon$	$0.1 \times 10^{-3}$	$0.1 \times 10^{-1}$
Reynolds number $Re_s$	700	700 - 4000

*i.e.*  $X/R_s = 2.89 - 9.46$ .

### 3. Simulation

A cylindrical coordinate system  $(r, \theta, z)$  was specified for the side branch (**Figure 1**) with corresponding velocity components  $(u, v, w)$ . The governing equations for the incompressible viscous fluid flow are the Navier Stokes equations,

$$\frac{\partial \mathbf{u}}{\partial x} + (\mathbf{u} \cdot \text{grad}) \mathbf{u} = -\text{grad } p + \frac{1}{Re_s} \Delta^2 \mathbf{u} \quad (2)$$

and the continuity equation,

$$\text{div } \mathbf{u} = 0 \quad (3)$$

where the dimensional variables  $(u, v, w)$ ,  $(r, \theta, z)$  and  $(X, Y, Z)$  are normalized using mean velocity  $U_s = 8 \times 10^{-2}$  m/s and radius of  $R_s = 7 \times 10^{-3}$  m in the side branch. Here, the kinematic viscosity and the density of the working fluid are  $\nu = 1.58 \times 10^{-6}$  m<sup>2</sup>/s and  $\rho = 1830$  kg/m<sup>3</sup>, respectively.

In the following numerical simulation, the steady flow is first obtained, and then an unsteady flow simulation was performed with the upstream boundary condition, in which the velocity field rotates around the axis of the side branch with a small angle around the axis of the side branch.

$$\mathbf{u}(r, \theta, 0) = \mathbf{u}_0(r, \theta + \Delta\theta) \quad (4)$$

As depicted in **Figure 3(c)**, the upstream boundary condition describes periodic oscillations with small angular variation,

$$\Delta\theta = \Delta\theta_0 \sin \pi St_s t \quad (5)$$

The amplitude of the rotation angle  $\Delta\theta_0$  is set to  $\pi/180$  ( $1^\circ$ ), and the frequency equals the empirical value observed in the experiment,  $St_s = 1.03$  ( $f = 6$  Hz) [18]. A time-dependent simulation was performed with the initial condition of the previous steady flow result until a steady oscillating flow was obtained.

The free-stream condition is applied at the downstream boundary. Thus, the flow instability in the side branch was generated numerically as follows. The time-dependent simulation was performed with the initial condition until a steady oscillating flow was obtained.

The discretized representations of the relevant equations were obtained

through the control volume method, and solved using an iterative algorithm employed in the original code similar to SIMPLER method developed by Patanker [20]. The features of the present solution procedure [21] are summarized as follows. The convective derivative terms are discretized through the consistently reformed QUICK scheme, which guarantees continuity of momentum flux during each iteration and significantly improves numerical stability [22]. The modified strongly implicit procedure of Schneider and Zedan is employed to solve the linearized penta-diagonal matrix equations [23]. In discretizing the local derivative term, the second-order accurate three-time-level scheme is employed [24].

The numerical settings are listed in **Table 1**. Parameter values for grid A such as the grid spacing and the length of the computational domain are determined from a preliminary simulation using grid B. The numerical simulations were carried out for both grids A and B. The criterion for each velocity is the convergence  $\varepsilon$ . Comparing of the amplification degree in grid A with that in grid B as described below, there is little difference between grid A and grid B. So, we primarily carried out to simulate in grid A with coarse mesh and uniform grid.

The amplification degree is defined as the ratio of  $(U_{rms})_{max}$  within  $X/R_S = 2.89 - 9.46$  to  $(U_{rms})_0$  at the section  $S_3$  as follows,

$$U_{rms} = \sqrt{\frac{1}{TA} \int_T \int_A |u'|^2 da dt} \quad (6)$$

where  $T$  and  $A$  are period and cross sectional area of side branch, respectively. When various frequencies, specifically, 0.1 Hz and 1 Hz to 12 Hz in steps of 1Hz, were set for the perturbation at the upstream boundary section, the degree of amplification in the spatial change of axial velocity across each cross section examined downstream in the side branch depended on the given frequency. When the ratio of the amplification degree  $(U_{rms})_{max}$  of at each section to  $(U_{rms})_0$  at section  $S_3$  converged within 5% of the maximum amplification degree found under various frequencies as described above, the given frequency was regarded to be reasonable. This is the major criterion for the convergence in the present numerical simulation.

## 4. Results and Discussion

A time dependent simulation was performed with a null velocity field as an initial condition. After the transient flow diminished, the flow solution converged onto a steady state, *i.e.* the flow oscillation appearing in experiments was not reproduced in this simulation. The fixed upstream velocity boundary condition has probably stabilized the flow in the side branch. For this reason, the effect of a small perturbation given in (4) was examined in relation to the stability of the flow field.

Under the periodic oscillations imposed on the upstream boundary condition as described above, the oscillation in the axial velocity component at the off-axis

point  $(X/R_s, Z/R_s) = (0, 0.25)$  for three axial sections  $S_3$ ,  $S_5$  and  $S_7$  ( $X/R_s = 2.89, 4.32, 5.75$ ) was shown in **Figure 4(a)** and **Figure 4(b)**. This instant at  $t = 12.7$  corresponds when the oscillation of the axial velocity at the point is a minimum. It is sure that the velocity change, *i.e.* amplitude, is small in section  $S_3$  and a little large in section  $S_5$ . It becomes much larger in section  $S_7$ . Further downstream of section  $S_7$ , the amplification attenuates asymptotically. Thus, the spatial amplification and section of velocity relates to the flow instability. The small periodic oscillation given at the upstream boundary  $S_3$  is substantially amplified at the downstream location  $S_7$  with a phase lag of  $0.21\pi$  rad which is calculated from the time difference  $\Delta t = 0.2$ , *i.e.*  $t = 12.7$  and  $t = 12.9$ , of the minimum velocity in sections  $S_3$  and  $S_7$ , respectively. As one period is 1.9, the phase lag is  $2\pi \times 0.2/1.9 = 0.21\pi$ . This one period of 1.9 corresponds to the periodic frequency of  $f = 6.00$  Hz, *i.e.*  $St_s = 1.05$ , which agrees well with the experimental results of 1.03 [18].

Contours plots of the secondary velocity vector and the iso-axial velocity contours at the downstream sections  $S_5$  and  $S_7$  ( $X/R_s = 4.32$  and  $5.75$ ) at  $t = 12.7$  (**Figure 5**) show a pair of small vortices in the downstream section  $S_5$  ( $X/R_s = 4.32$ ), which are also seen in the upstream boundary, moving toward the near wall while another pair of slightly stronger vortices grew larger; the iso-axial velocity contours are a little asymmetric. Section  $S_7$  ( $X/R_s = 5.75$ ) further downstream features two pairs of small and large vortices merging to form one pair of large vortices. Significant asymmetry is indicated in the axial velocity distribution; also, the iso-axial velocity contour is asymmetric because of flow instability, *i.e.* the small periodic velocity oscillation introduced in the upstream boundary has amplified downstream. The current simulation results at the sections  $S_5$  and  $S_7$  qualitatively agree with the experimental results (**Figure 6**), respectively [19] although the secondary velocity of the experimental result is a little bigger than the numerical result. Simultaneously, the flow instability was induced along the shearing separation layer (see **Figure 7**) at  $X/R_s = 3.17$  immediately downstream

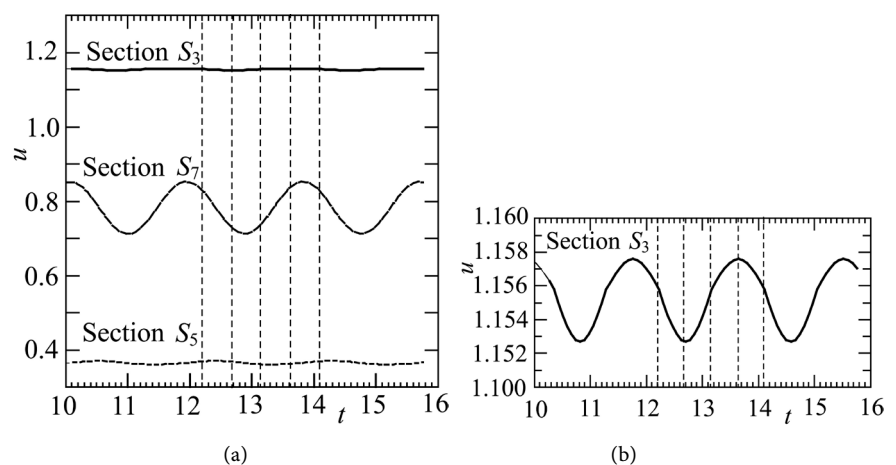


**Figure 4.** Time variation of axial velocity in sections  $S_3$ ,  $S_5$  and  $S_7$  at representative point ( $Y/R_s = 0.0, Z/R_s = 0.25$ ). (a) Axial velocity in sections  $S_3$ ,  $S_5$  and  $S_7$ ; (b) Magnified axial velocity in section  $S_3$ .

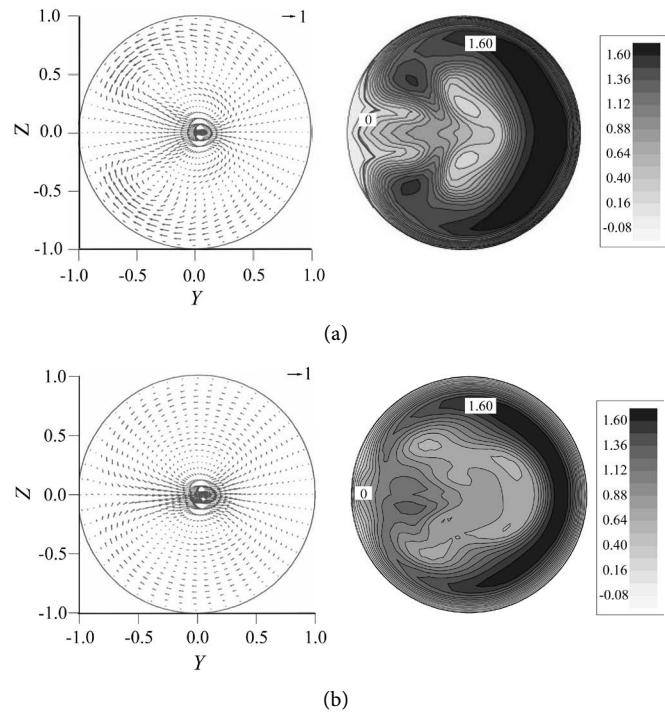


**Figure 5.** Secondary velocity vector plots and iso-axial velocity contours at  $t = 12.7$ . (a) Section  $S_5$ ; (b) Section  $S_7$ .

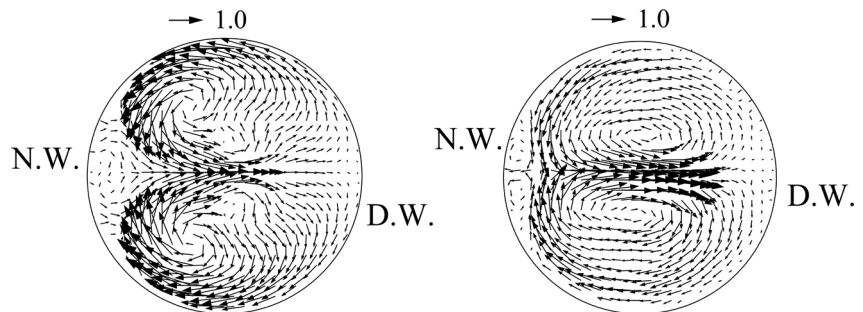


**Figure 6.** Secondary velocity vector measured in PIV [18]. Left and right sides denote at sections  $S_5$  and  $S_7$ , respectively.

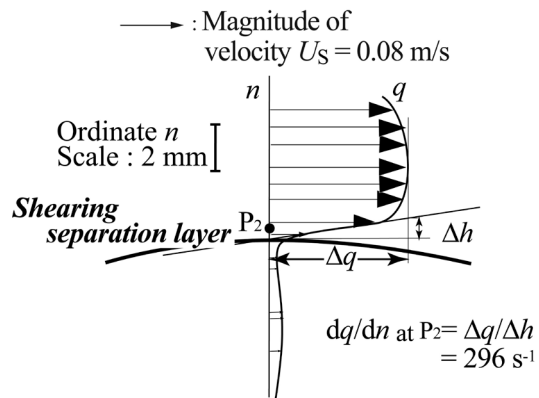


**Figure 7.** Tangential velocity profile across shearing separation layer at section  $X/R_5 = 3.17$  (Shear rate downstream of side branch =  $47 \text{ s}^{-1}$ ) [19].

from section  $S_3$  [19]. The shear-rate ( $296 \text{ s}^{-1}$ ) at this layer is 6 times larger than that ( $47 \text{ s}^{-1}$ ) at the tube wall downstream of the side branch; the tangential velocity profile indicates a clear inflection point. This is one feature associated with the flow instability in the side branch of T-junction, which is one kind of Kelvin-Helmholtz instabilities. In the upper half of **Figure 3(a)** and **Figure 3(b)**, there exist two counter-clockwise vortices, which generate a small vortex at the near wall and a little strengthening large vortex with the same rotational sense. Therefore, the high-shear-rate at the interface between these two vortices is another feature of this flow instability. Two pairs of vortex in the experiment look like those in curved bend [25] [26]. However, two pairs of vortex in the present result as shown in **Figure 3(a)** is fundamentally different from those in the curved bend, which these vortices rotate without same rotational sense and hence there is no friction at the interface between each vortex.

The range of Strouhal number  $St_s$ , *i.e.* oscillating frequency, in the present simulation approximately agrees with that obtained in experiment (**Figure 8**) in the range of  $St_s = 0.9 - 1.1$ , although there is a little deviation between the simulation and the experiment. Indeed, the observed oscillation depends on the amplification of flow instability in the side branch.

The time average WSS  $\tau_{uw}$  in the distal wall in **Figure 9(a)** is much larger than that in the near wall; moreover, WSS  $\tau_{uw}$  in the section  $S_3$  is globally larger than that in the downstream region. The root mean square (RMS) of WSS  $\tau_{uw-rms} = 0.9$  at  $X/R_s = 8.5$  in the downstream region as shown in **Figure 9(b)** is much higher than that of 0.2 at  $X/R_s = 3.2$  downstream of section  $S_3$ . This difference in  $\tau_{uw-rms}$  is closely related to the flow instability that is amplified in the downstream region. Furthermore, the amplitude of the resultant WSS  $\tau_{uw-amp} = 1.75$  at the near wall  $X/R_s = 6.5$  denoted by A and  $\tau_{uw-amp} = 2.50$  at the distal wall  $X/R_s = 8.5$  denoted by B are large in **Figure 9(c)**.

## 5. Conclusion

The mechanism for flow instability in the side branch of a T-Junction in steady laminar flow was clarified using a periodic velocity perturbation introduced as

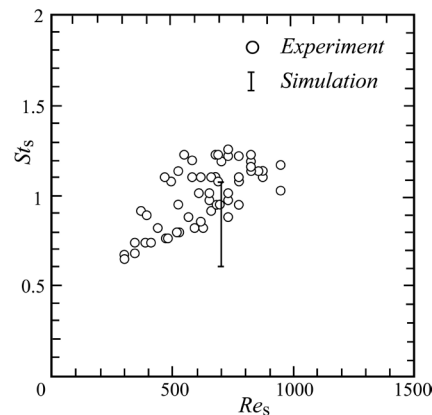


**Figure 8.** Reynolds number  $Re_s$ , versus, Strouhal number  $St_s$ .

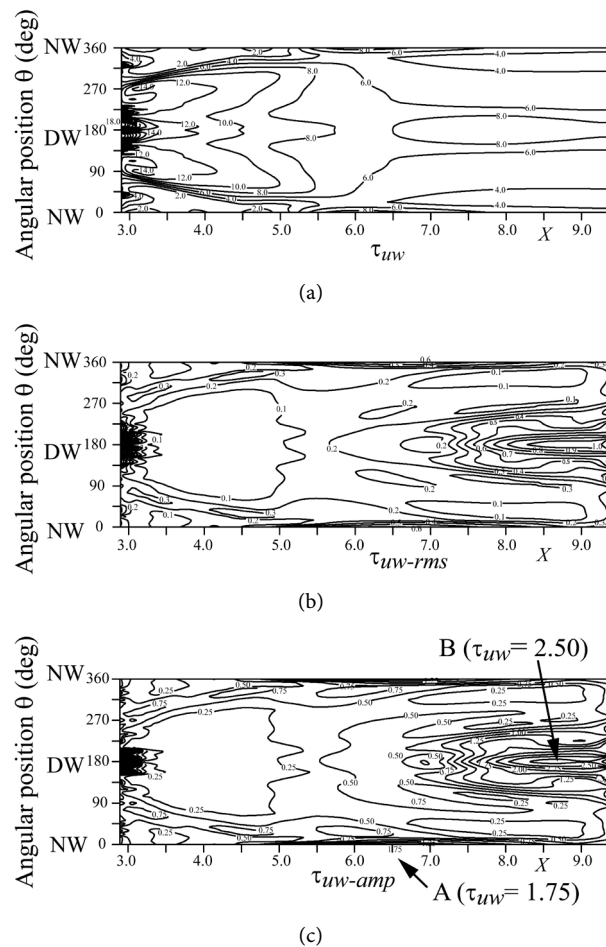


**Figure 9.** Contours of time average, RMS and amplitude of resultant WSS  $\tau_{uw}$ . (a) Time average of WSS; (b) RMS of WSS; (c) Amplitude of resultant WSS.

an upstream boundary condition in a numerical simulation. The simulation result qualitatively agrees with experimental measurements. The spatial amplification accompanied with the flow instability in the side branch by numerical simulation explains the occurrence of the velocity oscillation observed in the experiment. Therefore, this periodic oscillation motion is a universal phenomenon in the side branch of a T-junction.

## Acknowledgements

The authors thank Mr. Takashi Fujiwarain Chiba University for suggestions concerning data processing.

In this study, the authors cited **Figure 3(a)** from Yamaguchi, R. *et al.*, “Variation of Wall Shear Stress and Periodic Oscillations Induced in the Right-Angle Branch during Laminar Steady Flow”, **127** (2005) [18] and **Figure 6** and **Figure 7** from Tanaka, G. *et al.*, “Fluid Vibration Induced by High-Shear-Rate Flow in a T-Junction”, **138** (2016) [19] published by ASME J. Fluids Eng., after getting the permission of copyright.

The authors declare no conflicts of interest.

## References

- [1] Karino, T., Kwong, H.H.M. and Goldsmith, H.L. (1979) Particle Flow Behavior in Models of Branching Vessels: I Vortices in 90° T-Junctions. *Biorheology*, **16**, 231-248.
- [2] Liepsch, D., Poll, A., Strigberger, J., Sabbah, H.N. and Stein, P.D. (1989) Flow Visualization Studies in a Mold of the Normal Human Aorta and Renal Arteries. *ASME Journal of Biomechanical Engineering*, **111**, 222-227. <https://doi.org/10.1115/1.3168369>
- [3] Perktold, K. and Peter, R. (1990) Numerical 3D-Simulation of Pulsatile Wall Shear Stress in an Arterial T-Bifurcation Model. *Journal of Biomechanical Engineering*, **12**, 2-12. [https://doi.org/10.1016/0141-5425\(90\)90107-X](https://doi.org/10.1016/0141-5425(90)90107-X)
- [4] Yung, C.N., De Witt, K.J. and Keith Jr., T.G. (1990) Three-Dimensional Steady Flow through a Bifurcation. *ASME Journal of Biomechanical Engineering*, **112**, 189-197. <https://doi.org/10.1115/1.2891171>
- [5] Valen-Sendstad, K., Mardal, K.-A., Mortensen, M., Reif, B.A.P. and Langtangen, H.P. (2011) Direct Numerical Simulation of Transitional Flow in a Patient-Specific Intracranial Aneurysm. *Journal of Biomechanics*, **44**, 2826-2832. <https://doi.org/10.1016/j.jbiomech.2011.08.015>
- [6] Il'ichev, A.T. and Fu, Y.-B. (2012) Stability of Aneurysm Solutions in a Fluid-Filled Elastic Membrane Tube. *Acta Mechanica Sinica*, **28**, 1209-1218. <https://doi.org/10.1007/s10409-012-0135-2>
- [7] Baek, H., Jayaraman, M.V., Richardson, P.D. and Karniadakis, G.E. (2010) Flow Instability and Wall Shear Stress Variation in Intracranial Aneurysms. *Journal of the Royal Society Interface*, **7**, 967-988. <https://doi.org/10.1098/rsif.2009.0476>
- [8] Baes, A.J., Dooly, D.J., Schroter, R.C., Cetto, R., Calmet, H., Gambaruto, A.M., Tolly, N. and Houzeaux, G. (2015) Dynamics of Airflow in a Short Inhalation. *Journal of the Royal Society Interface*, **12**, 20140880.
- [9] Dooly, D., Taylor, D.J., Franke, P. and Schroter, R.C. (2008) Experimental Investigation of Nasal Airflow. *Journal of Engineering in Medicine*, **222**, 439-453. <https://doi.org/10.1243/09544119JEIM330>
- [10] Balint, T.S. and Lucey, A.D. (2005) Instability of a Cantilevered Flexible Plate in Viscous Channel Flow. *Journal of Fluids and Structures*, **20**, 893-912. <https://doi.org/10.1016/j.jfluidstructs.2005.05.005>
- [11] Brown, G.L. and Roshko, A. (1974) On Density Effects and Large Structure in Turbulence Mixing Layers. *Journal of Fluid Mechanics*, **64**, 775-816. <https://doi.org/10.1017/S002211207400190X>
- [12] Tani, I. (1964) Low-Speed Flows Involving Bubble Separation. *Progress in Aerospace Sciences*, **5**, 79-103.
- [13] Sarohia, V. (1977) Experimental Investigation of Oscillations Flows over Shallow Cavities. *AIAA Journal*, **15**, 984-991. <https://doi.org/10.2514/3.60739>
- [14] Rockwell, D. and Naudascher, E. (1978) Review: Self-Sustaining Oscillations of Flow past Cavities. *Journal of Fluids Engineering*, **100**, 152-165. <https://doi.org/10.1115/1.3448624>
- [15] Sherwin, S.J. and Blackburn, H.M. (2005) Three-Dimensional Instabilities and Transition of steady and Pulsatile Axisymmetric Stenotic Flows. *Journal of Fluid Mechanics*, **533**, 297-327. <https://doi.org/10.1017/S0022112005004271>
- [16] Yamaguchi, R., Mashima, T. and Takahashi, Y. (1997) Separated Secondary Flow and Wall Shear Stress in Side Branch of Right Angle Branch. ASME Paper No. 3303.

- [17] Yamaguchi, R., Shigeta, M., Kudo, S. and Hayase, T. (2000) Wall Shear Stress and Periodical Oscillation Induced in Side Branch at Right Angle Branch in Laminar Steady Flow. ASME Paper No. 11085.
- [18] Yamaguchi, R., Mashima, T., Amagai, H., Fujii, H., Hayase, T. and Tanishita, K. (2005) Variation of Wall Shear Stress and Periodic Oscillations Induced in the Right-Angle Branch during Laminar Steady Flow. *Journal of Fluids Engineering*, **127**, 1013-1020. <https://doi.org/10.1115/1.1852480>
- [19] Tanaka, G., Yamaguchi, R., Liu, H. and Hayase, T. (2016) Fluid Vibration Induced by High-Shear-Rate Flow in a T-Junction. *Journal of Fluids Engineering*, **138**, Article ID: 081103. <https://doi.org/10.1115/1.4032935>
- [20] Patanker, S.V. (1980) Numerical Heat Transfer and Fluid Flow. Hemisphere, Washington DC, New York.
- [21] Hayase, T., Humphrey, J.A.C. and Greif, R. (1990) Mini Manual for ROTFLO2. Department of Mechanical Engineering Report, FM-90-1, University of California, Berkeley.
- [22] Hayase, T., Humphrey, J.A.C. and Greif, R. (1992) A Consistently Formulated QUICK Scheme for Fast and Stable Convergence Using Finite-Volume Iterative Calculation Procedures. *Journal of Computational Physics*, **98**, 108-118.
- [23] Schneider, G.E. and Zedan, M. (1981) A Modified Strongly Implicit Procedure for Numerical Solution of Field Problems. *Numerical Heat Transfer*, **4**, 1-19. <https://doi.org/10.1080/01495728108961775>
- [24] Fletcher, C.A. (1988) Computational Techniques for Fluid Dynamics. Springer-Verlag, Berlin, Vol. 1, 302.
- [25] Ault, J.T., Chen, K.K. and Stone, H.A. (2015) Downstream Decay of Fully Developed Dean Flow. *Journal of Fluid Mechanics*, **777**, 219-244. <https://doi.org/10.1017/jfm.2015.353>
- [26] Tada, S., Oshima, S. and Yamane, R. (1990) Flow Pattern of the Fully Developed Pulsatile Flow in a Curved Pipe. *Transactions of the JSME*, **56**, 3240-3247. (In Japanese)

## Nomenclature

- $f$ : frequency of fluid vibration  
 $L$ : streamwise length of simulation domain  
 $n$ : coordinate normal to shearing separation layer  
 $Q_S$ : flow rate through side branch  
 $Q_T$ : flow rate through trunk  
 $q$ : tangential velocity along shearing separation layer  
 $Re_S = 2R_S U_S / \nu$ : Reynolds number based on variables of side branch  
 $Re_T = 2R_T U_T / \nu$ : Reynolds number based on variables of trunk  
 $R_S$ : radius of side branch= 7 mm  
 $R_T$ : radius of trunk= 12.25 mm  
 $(r, \theta, z)$ : cylindrical coordinate defined in side branch  
 $St_S = 2fR_S / U_S$ : Strouhal number based on variables of side branch  
 $t = \hat{t} / (R_S / U_S)$ : dimensionless time  
 $\hat{t}$ : dimensional time  
 $U_{rms}$ : root mean square root of axial velocity  
 $(U_{rms})_0$ : root mean square root of axial velocity at section  $S_3$   
 $U_S$ : mean velocity in side branch  
 $U_T$ : mean velocity in trunk  
 $(u, v, w)$ : velocity component in  $(r, \theta, z)$  coordinate direction, respectively  
 $(u', v', w')$ : velocity fluctuation of each velocity  
 $(X, Y, Z)$ : Cartesian coordinate defined in the whole right angle branch  
 $\tau_{uw}^*$ : non-dimensional resultant wall shear stress [=  $\tau_{uw}^* / (4\rho\nu U_T / R_T)$ ]  
 $\tau_{uw}^*$ : dimensional resultant wall shear stress  
 $\nu$ : kinematic viscosity of working fluid  
 $\rho$ : density of working fluid